

LONG-TERM VARIATIONS IN THE GROWTH AND DECAY RATES OF SUNSPOT GROUPS

J. JAVARAI AH

© Springer ●●●

Abstract Using the combined Greenwich (1874–1976) and Solar Optical Observatories Network (1977–2009) data on sunspot groups, we study the long-term variations in the mean daily rates of growth and decay of sunspot groups. We find that the minimum and the maximum values of the annually averaged daily mean growth rates are $\approx 52\%$ day⁻¹ and $\approx 183\%$ day⁻¹, respectively, whereas the corresponding values of the annually averaged daily mean decay rates are $\approx 21\%$ day⁻¹ and $\approx 44\%$ day⁻¹, respectively. The average value (over the period 1874–2009) of the growth rate is about 70% more than that of the decay rate. The growth and the decay rates vary by about 35% and 13%, respectively, on a 60-year time-scale. From the beginning of Cycle 23 the growth rate is substantially decreased and near the end (2007–2008) the growth rate is lowest in the past about 100 years. In the extended part of the declining phase of this cycle, the decay rate steeply increased and it is largest in the beginning of the current Cycle 24. These unusual properties of the growth and the decay rates during Cycle 23 may be related to cause of the very long declining phase of this cycle with the unusually deep and prolonged current minimum. A ≈ 11 -year periodicity in the growth and the decay rates is found to be highly latitude and time dependent and seems to exist mainly in the $0^\circ - 10^\circ$ latitude interval of the southern hemisphere. The strength of the known approximate 33–44 year modulation in the solar activity seems to be related to the north-south asymmetry in the growth rate. Decreasing and increasing trends in the growth and the decay rates indicate that the next 2–3 solar cycles will be relatively weak.

1. Introduction

Magnetic flux, in the form of large flux tubes, emerges to the surface—presumably from near the base of the convection zone (where the dynamo process is believed to be taking place)—and responsible for sunspots and other solar active phenomena (see Rosner and Weiss, 1992; Gough, 2010). A sunspot lasts from a few hours to several weeks. The typical sizes of sunspots range from 10 msh (millionth of

Indian Institute of Astrophysics, Bangalore-560 034, India.
email: jj@iiap.res.in

the solar hemisphere $\approx 3 \times 10^6 \text{ km}^2$) to 10^3 msh. Although individual sunspots are common, the majority of sunspots are parts of groups. Spot groups are often large and complex. The daily area of a spot (or spot group) is one of the most important parameters used to describe the spot (or spot group) development. The area of a spot (or spot group) is closely connected with the magnetic flux of the spot (or spot group) (130 msh area $\approx 10^{22}$ Mx magnetic flux, *e.g.*, see Wang and Sheeley, 1989). That is, the development of the spot (or spot group) area reflects the development of the solar magnetic field. Therefore, the increase/decrease in the areas of spots or spot groups, *i.e.*, the growth/decay of spots or spot groups, can affect significantly the strength, configuration and topology of the magnetic structure in the solar atmosphere. Hence, the studies of growth and decay of sunspots or sunspot groups are important for understanding configuration and topology of the magnetic structure on the solar surface, the solar variability and the underlying mechanism of it. Several such studies have been made and many characteristics of the growth and decay of the spot groups are found (see Lustig and Wöhl, 1995; Hathaway and Choudhary, 2008).

Howard (1992a,1992b) analyzed Mt. Wilson sunspot and sunspot group data during 1917–1985 and determined many properties of the day-to-day changes in the sunspot umbral areas (spot growth/decay). Howard (1992a) also studied the variations in the annual averages of the umbral area increases, but no systematic variations are found. In the present study we analyze a large data set of sunspot groups and attempt to detect the long-term variations in daily rates of growth and decay of sunspot groups.

In the next section we describe the methodology and the data analysis. In Section 3 we present the results. In Section 4 we draw conclusions and briefly discuss the implications of them on the long-term solar variability.

2. Methodology and data analysis

Here we have used the combined Greenwich (1874–1976) and Solar Optical Observation Network (SOON) (1977–2009) sunspot group data, which are taken from David Hathaway’s website <http://solarscience.msfc.nasa.gov/greenwch.shtml>. These data included the observation time (the Greenwich data contain the date with the fraction of the day, in the SOON data the fraction is rounded to 0.5 day), heliographic latitude (ϕ) and longitude (L), central meridian distance (CMD), and corrected umbra and whole-spot areas (in msh), etc., of the spot groups for each day of observation. The positions of the groups are geometrical positions of the centers of the groups.

The Greenwich data have been compiled from the majority of the white light photographs which were secured at the Royal Greenwich Observatory and at the Royal Observatory, Cape of Good Hope. The gaps in their observations were filled with photographs from other observatories, including the Kodaikanal Observatory, India. The SOON data included measurements made by the United States Air Force (USAF) from the sunspot drawings of a network of the observatories that has included telescopes in Boulder, Colorado; Hawaii; etc. David Hathaway scrutinized the Greenwich and SOON data and produced a reliable

continuous data series from 1874 up to date (also see Hathaway and Choudhary, 2008). In case of SOON data, we increased the area by a factor of 1.4. David Hathaway found this correction was necessary to have a combined homogeneous Greenwich and SOON data (see the aforementioned website of David Hathaway.)

The method of analysis is similar to that in Howard (1992a). Howard used daily umbral areas of the spots measured in Mt. Wilson Observatory during the years 1917–1985. We have used the corrected daily whole-spot areas (umbral value + penumbral value) of spot groups (A). A spot group is included when the observations of it are available for two or more consecutive days. The daily rate of change of the area ($\frac{\Delta A}{\Delta t}$) of a spot group is computed using the differences between the epochs of its observation in consecutive days and between the corrected whole-spot areas of the spot group at these epochs. That is,

$$\frac{\Delta A}{\Delta t} = \frac{A_n - A_{n-1}}{t_n - t_{n-1}}, \quad (1)$$

where t is the epoch of observation during the life time (T) of a spot group and $n = 2, 3, \dots, T$. Positive and negative values of $\frac{\Delta A}{\Delta t}$ correspond to the daily rates of growth (G) and decay (D) of a spot group, respectively. The percentage of growth ($\%G$) and decay ($\%D$) are calculated as $(G \times 100)/A_{n-1}$ and $(D \times 100)/A_{n-1}$, respectively. The mean values ($\overline{\%G}$ and $\overline{\%D}$) of $\%G$ and $\%D$ in a given time interval are calculated as follows:

$$\overline{\%G} = \frac{1}{k} \Sigma \%G_i \quad \text{and} \quad \overline{\%D} = \frac{1}{m} \Sigma \%D_j, \quad (2)$$

where $i = 1, 2, \dots, k$ and $j = 1, 2, \dots, m$; k and m are the number of data points of $\%G$ and $\%D$, respectively, in the interval. It should be noted that obviously more contributions to $\overline{\%G}$ and $\overline{\%D}$ are coming from the spot groups before and after reaching their maximum areas, respectively.

The data on the recurrent and the non-recurrent spot groups are combined. The first and the subsequent disc passages of the recurrent spot groups are treated as independent groups. Therefore, the life time of a spot group is ≤ 12 days. As in the case of our earlier papers (Javaraiah 2010, and references therein), here we have taken the following precaution which reduces substantially the uncertainties in the derived results (Ward, 1966; Javaraiah and Gokhale, 1995): We have excluded the data corresponding to the $|CMD| > 75^\circ$ on any day of the spot group life span. This reduced the error due to the foreshortening effect. Further, we excluded the data corresponding to the ‘abnormal’ motions, *e.g.* displacements exceeding 3° day^{-1} in the longitude or 2° day^{-1} in the latitude. This reduces uncertainties in $\overline{\%G}$ and $\overline{\%D}$ removing those which were incorrectly identified. For the sake of readers convenience, in Table 1 and Figure 1 we have demonstrated the determination of $\%G$ and $\%D$ for one spot group: NOAA/USAF spot group no. 2288, observed during the days 18.5–29.5 of February 1980 (Note: Greenwich sunspot group number through 1976; NOAA/USAF group number after 1976). If there is only this spot group in the given time interval (say in one year, 1980), then $\overline{\%G}$ is 105.7, determined from the five values of $\%G$ at the epochs 19.5–20.5, 20.5–21.5, 21.5–22.5, 24.5–25.5, and 26.5–27.5 during the life time of this spot group, and $\overline{\%D}$ is 22.4,

Table 1. The data of the spot group, NOAA/USAF spot group no. 2288, observed during the days 18.5–29.5 of February 1980. A positive and a negative value of $\frac{\Delta A}{\Delta t}$ (differences of A on consecutive days) represent the growth rate (G) and decay rate (D) respectively.

t_n	L	ϕ	CMD	A	$\frac{\Delta A}{\Delta t}$	% G or % D
18.5	319.5	13.0	-67.0	10	10	100.0
19.5	317.4	10.0	-56.0	20	70	350.0
20.5	319.2	9.0	-41.0	90	60	66.7
21.5	320.0	10.0	-27.0	150	150	100.0
22.5	319.9	11.0	-14.0	300	-20	-6.7
23.5	320.7	10.0	0.0	280	-10	-3.5
24.5	320.5	10.0	13.0	270	10	3.7
25.5	320.4	10.0	26.0	280	-160	-57.1
26.5	320.2	10.0	39.0	120	10	8.3
27.5	321.0	11.0	53.0	130	-90	-69.2
28.5	325.9	10.0	71.0	40	0	0.0
29.5 ^a	327.7	8.0	86.0	40		

^a indicates that this day data are not used here due to $CMD > 75^\circ$.

determined from the three values of % D at the epochs 22.5–23.5, 23.5–24.5, and 25.5–26.5. The standard errors of these mean values are $\sigma_g/\sqrt{(k)} = 63.9$ and $\sigma_d/\sqrt{(m)} = 17.3$, where σ_g and σ_d are the standard deviations correspond to % G and % D , respectively. The value of % G at the epoch 18.5–19.5 is not considered because $\frac{\Delta\phi}{\Delta t} > 2^\circ \text{ day}^{-1}$ and the value of % D at the epoch 27.5–28.5 is not considered because $\frac{\Delta L}{\Delta t} > 3^\circ \text{ day}^{-1}$ and $\frac{\Delta\phi}{\Delta t} > 2^\circ \text{ day}^{-1}$. The value at the epoch 28.5–29.5 is not considered because the CMD at the epoch 29.5 is $> 75^\circ$.

Hathaway and Choudhary (2008) analyzed the combined Greenwich and SOON data and found that the decay rates of the spot groups of Cycles 21–23 are much larger than those of Cycles 12–20. We noticed that some daily data records, particularly in the data during recent cycles (*i.e.*, in the SOON dataset), contain the zeros for the whole-spot group area. We excluded all those unrealistic data records, *i.e.*, we have excluded the data correspond to the whole-spot area equal to zero in any day during the life time of the spot group, because we find that presence of these unrealistic data yields large values for the derived decay rates.

We determined the variations in the mean percentage growth and decay rates (% G and % D) of the spot groups in the whole disk, in the northern and the southern hemispheres, and also in the separate 10° latitude intervals. The variations in % G and % D of the spot groups in the whole disk are determined from the yearly data and for the spot groups in a whole hemisphere the variations are determined by binning the data into 3- and 4-year moving time intervals (MTIs) that are successively shifted by one year during the period 1974–2009, for the sake of better statistics. In case of the separate 10° latitude intervals, we have used only 4-year MTIs because in a shorter than 4-year interval the data

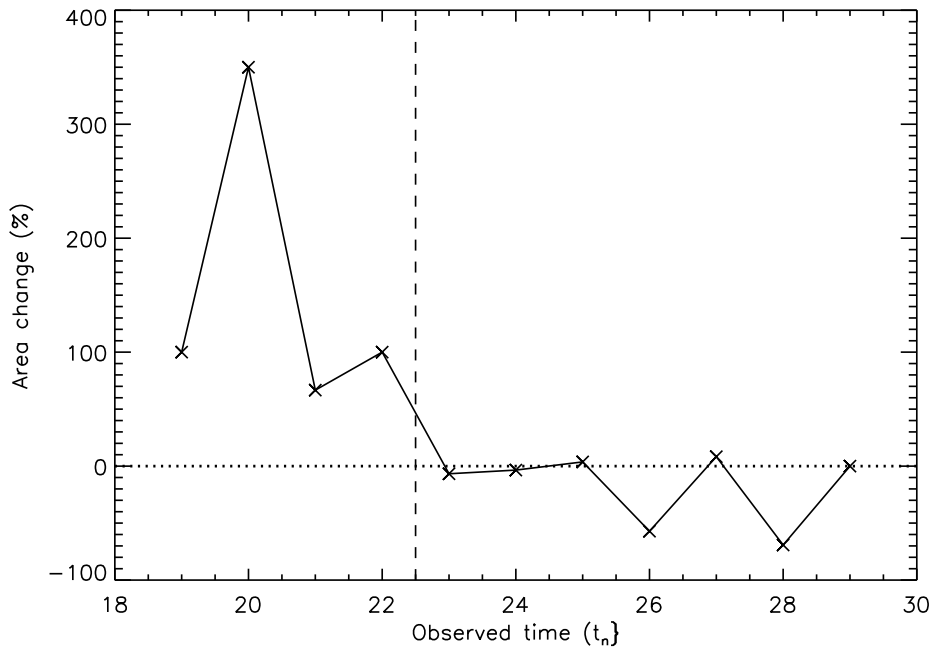


Figure 1. Plot of the percentage area change in the consecutive days during the life time of the spot group, NOAA/USAF spot group no. is 2288, observed during the days 18.5–28.5 of February 1980, *versus* time (middle epoch of a given consecutive day). The vertical dashed-line represents the epoch of the spot group maximum area. The positive and negative values correspond to the percentage growth day⁻¹ ($\%G$) and percentage decay day⁻¹ ($\%D$), respectively. The horizontal dotted-line is drawn at $\%G = \%D = 0$.

are found to be inadequate and the error bars are very large to plot the results, particularly during the cycles minima. The yearly as well as 3- and 4-MTIs time series of $\overline{\%G}$ and $\overline{\%D}$ have been corrected by replacing those values of $\overline{\%G}$ and $\overline{\%D}$ whose standard errors exceeded the 2.6 times (correspond to 99% confidence level) the corresponding median values with the average of the corresponding values and their respective two neighbors (in case of the beginnings of the time series it is the average of the values in the intervals 1 and 2 and in the endings it is the average of the values in the intervals $N - 1$ and N , where N is the size of the series). We determined the periodicities in $\overline{\%G}$ and $\overline{\%D}$ from the fast Fourier transform (FFT) power spectrum analysis of the corrected time series. The values of the periodicities are determined from the maximum entropy method (MEM). The time-dependencies in the periodicities in $\overline{\%G}$ and $\overline{\%D}$ are checked using Morlet wavelet analysis. The MEM and the wavelet analyses of $\overline{\%G}$ and $\overline{\%D}$ were carried out in a similar way as in the analyses of the mean meridional motions of the spot groups by Javaraiah (2010) and are briefly described below.

The lengths of the time series are inadequate to measure precisely the values of ≥ 11 -year periodicities in $\overline{\%G}$ and $\overline{\%D}$ from the FFT analysis. Hence, the uncertainties in the longer periodicities determined here from the FFT analysis are large. A different approach for determining the periodicities in a short time series with a higher accuracy is to compute the power spectrum using MEM.

MEM analysis is a parametric modeling approach to the estimation of the power spectrum of a time series. The method is data adaptive being used upon an autoregressive modeling process. An important step in this method is the optimum selection of the order M of the autoregressive process, which is the number of immediately previous points that have been used in the calculation of a new point. If M is chosen too low the spectrum is over-smoothed and the high resolution potential is lost. If M is chosen too high, frequency shifting and spontaneous splitting of the spectral peaks occur. The MEM code which we have used here takes the values for M in the range $(N/3, N/2)$ (Ulrych and Bishop, 1975) or $2N/\ln(2N)$ (Berryman, 1978). In order to find the correct values of the periodicities found in the FFT power spectrum, we have computed MEM power spectra choosing various values for M in the range $(N/3, N/2)$ and $2N/\ln(2N)$. We find that $M = N/3$ is suitable in the present MEM analysis, *i.e.*, in the derived spectra the peaks are considerably sharp and well separated.

Wavelet analysis provides both time-domain information and frequency-domain information simultaneously. We have used the wavelet IDL code provided by Ch. Torrence and G. P. Compo as described in Torrence and Compo (1998). Morlet wavelet consists of a complex exponential modulated by a Gaussian, $\exp(\omega_0 t/s)\exp(-t^2/(2s^2))$, where t is the time, s is the wavelet scale, and ω_0 is a non-dimensional frequency. A good temporal resolution is required to localize the power maxima in time and a good frequency resolution is required to determine the corresponding frequencies. A narrow (in time) function will have good time resolution but poor frequency resolution, while a broad function will have poor time resolution, yet good frequency resolution. For $\omega_0 = 6$ (used here), there are approximately three oscillations within the Gaussian envelope. According to Torrence and Compo (1998) it is convenient to write the scales as fractional powers of two: $s_j = s_0 2^{j\delta j}$, $j = 0, 1, \dots, J$ and $J = \delta j^{-1} \log_2(N\delta t/s_0)$, where s_0 is the smallest resolvable scale and J determines the largest scale. The s_0 should be chosen so that the equivalent Fourier period is approximately $2\delta t$. The choice of a sufficiently small δj depends on the width in spectral-space of the wavelet function. For the Morlet wavelet, $\delta j = 0.5$ is the largest value. The wavelet scale s is almost identical to the corresponding Fourier period, *i.e.*, the Morlet wavelet with $\omega_0 = 6$ gives $\lambda = 1.03s$, where λ is the Fourier period. Regions where edge effects become important, because of the finite length of the time series, are labeled as cone of influence (COI). The time series is padded with sufficient zeroes to bring the total length N up to the next power of two, limiting the edge effects and speeding up the Fourier transform (for more details see Torrence and Compo, 1998). In the present analysis $N = 136$, $\delta t = 1$ year, $s_0 = 2\delta t$, $\delta j = 0.105$ and $J = 58$. The wavelet spectra of $\overline{\%G}$ and $\overline{\%D}$ determined from the corrected annual data have reasonably good resolutions both in time and frequency.

3. Results

Figure 2 shows the variations in $\overline{\%G}$ and $\overline{\%D}$ (*cf.*, Equation 2) of the sunspot groups in the whole Sun, determined from the yearly spot group data during 1874–2009. Figure 3 shows the variations in $\overline{\%G}$ and $\overline{\%D}$ of the spot groups in

the northern and the southern hemispheres, determined from the data in 4-year MTIs (3-year MTIs series is not shown because it is found to be almost the same as that of 4-year MTIs series). Figures 4 and 5 show the variations in $\overline{\%G}$ and $\overline{\%D}$ of the spot groups in different 10° latitude intervals determined from the data in 4-year MTIs. To study the solar cycle variations in $\overline{\%G}$ and $\overline{\%D}$, in all of these figures we have also shown the variations in the sunspot activity. (Note: as per the definition of D , $\overline{\%D}$ has negative sign. For the sake of convenience we have plotted its absolute values.)

As can be seen in Figure 2, the minimum and the maximum values of $\overline{\%G}$ are ≈ 52 and ≈ 183 , respectively, and the corresponding values of $\overline{\%D}$ are ≈ 21 and ≈ 44 , respectively (we have given here the maximum and the minimum values in the corrected annual time series). The average value (over the period 1874–2009) of the growth rate is about 70% higher than that of the decay rate. Figure 6 shows the plots of the yearly mean values (correspond to the corrected annual time series) of $\overline{\%G}$ and $\overline{\%D}$ versus the year of the solar Cycles 12–23 (the point at year 9 belongs to the beginning year of the current Cycle 24 and the data are available only for the last four years of Cycle 11). To recognize and compare between the variations during individual cycles, the odd- and even-numbered cycles data are plotted with different colors, and different symbols are used for different pairs of the odd- and even-numbered cycles. In Figure 6(a) the overall spread in the data points of $\overline{\%G}$ is very large. Thus, the variations during different solar cycles highly differ (deviations from the mean variation are large in the cases of Cycles 15 and 20), suggesting that there is no statistically significant 11-year periodicity in $\overline{\%G}$. In the case of Cycle 20, in which the deviation is largest, there is a high anticorrelation between $\overline{\%G}$ and amount of activity. As can be seen Figure 6(b), the mean pattern of $\overline{\%D}$ suggests that $\overline{\%D}$ decreased from the beginnings of the cycles, reached minimum at 1–2 years after the maximum epochs, and then increased up to near the ends of the cycles. However, the spread in the data points of $\overline{\%D}$ is large before the epoch -2 and after the epoch 2. That is, there is a large ambiguity in the mean pattern. Thus, the 11-year cycle is not quite evident even in $\overline{\%D}$. The variations in $\overline{\%D}$ during a large numbers of the odd-numbered cycles seem to be little more closer to the mean variation than those of even cycles. However, the deviation from the mean variation is very large in the case of Cycle 21. In the case of Cycle 23, which is an anomalous cycle in the sense that the cycle pair 22,23 violated the Gnevyshev and Ohl rule (according to this rule a preceding even-numbered cycle is weaker than its following odd-numbered cycle), $\overline{\%G}$ decreased substantially from starting to near the beginning of the declining phase and then remained in the same low level for a long time, near the end it is smallest in the last about 100 years. In fact, it is close to the corresponding small value in the declining phase of Cycle 11. Interestingly, the length of the declining phase of Cycle 11 is also substantially long (it is longer than those of Cycles 12–22). In Cycle 23 the variation in $\overline{\%D}$ is close (less deviation) to the mean variation from the beginning year to ≈ 11 th year, but it strongly increased during the extended part of the declining phase (beyond the duration of the declining phase of a normal cycle) of this cycle and it is largest in the beginning of the current Cycle 24. These unusual properties of $\overline{\%G}$ and $\overline{\%D}$ in Cycle 23 may be related to the process

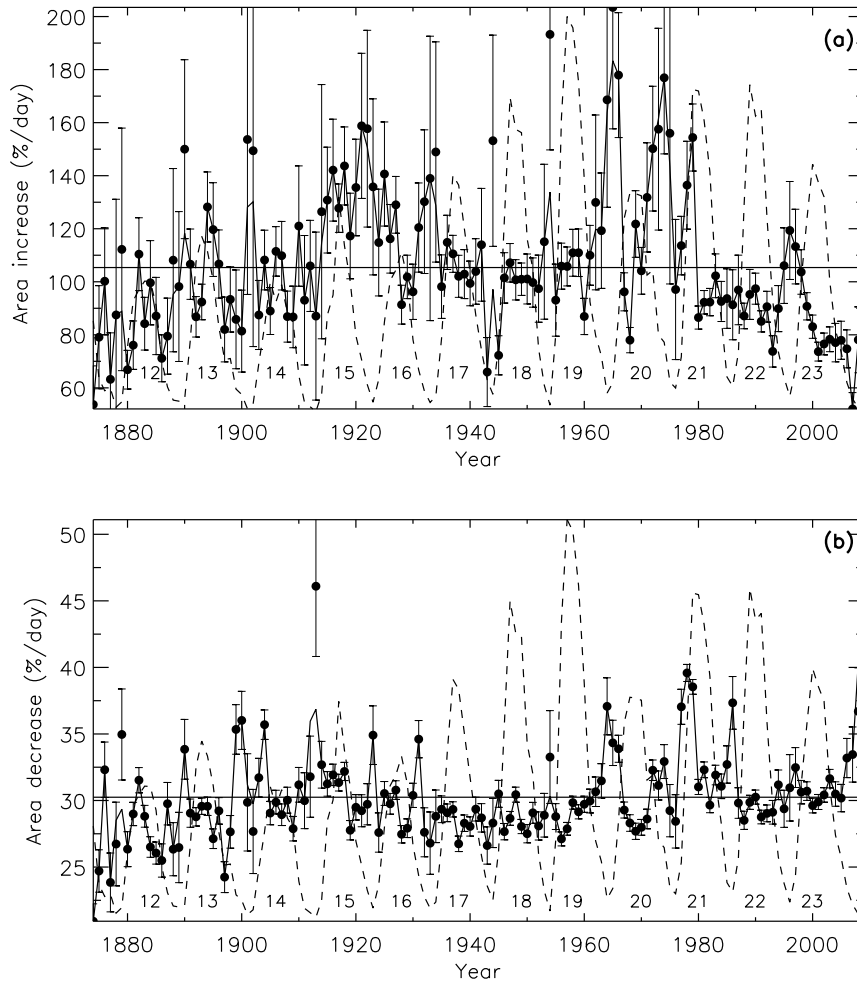


Figure 2. Plots of annual values of the mean percentage rates of the increase ($\overline{\%G}$, upper panel) and the decrease ($\overline{\%D}$, lower panel) in the daily area of the sunspot groups (*cf.*, Equation (2)) in the whole Sun *versus* time, during the period 1874–2009. The unconnected points represent the values which have a large uncertainty, *i.e.* standard error > 2.6. The dashed curve represents the annual variation in sunspot activity during 1874–2009. The Waldmeier cycle number is specified near the maximum epoch of each cycle.

which caused the very long decline phase of this cycle with the unusually deep and prolonged current minimum.

As can be seen Figures 2 and 3, the average values of $\overline{\%G}$ over the periods 1910–1940 and 1960–1980 seem to be larger than the corresponding average values over the periods 1874–1910, 1940–1960, and 1980–2008. Moreover, although there are fluctuations of several time scales, one can see the following trends: an increase in $\overline{\%G}$ from 1874 to 1920, a decrease from 1920 to 1940 and then an increase up to 1965, and again a decrease up to 2008. This pattern

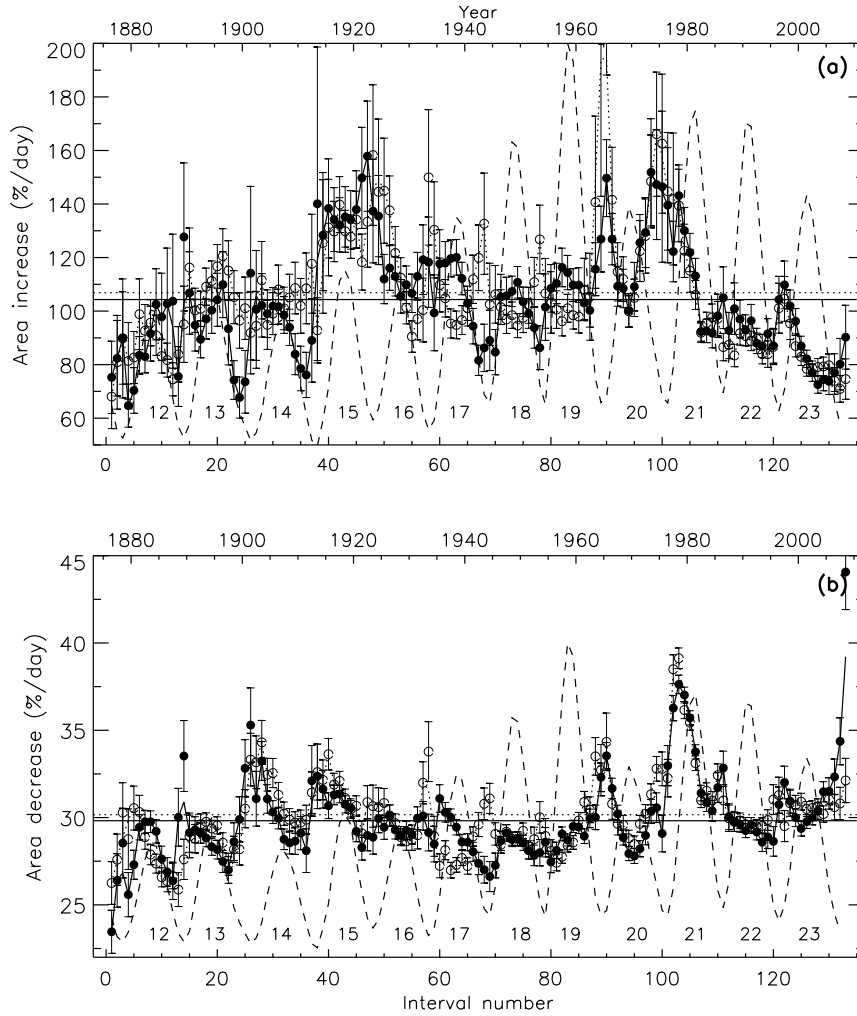


Figure 3. Variations in the mean percentage daily rates of increase ($\overline{\%G}$, upper panel) and decrease ($\overline{\%D}$, lower panel) in the area of the spot groups in the northern hemisphere (filled circle-solid curve) and the southern hemisphere (open circle-dotted curve) determined from 4-year MTIs, 1874–1877, 1875–1878, ..., 2006–2009. The unconnected points represent the values which have a large uncertainty, *i.e.* standard error > 2.6 . The dashed curve represents the variation of the sunspot number smoothed by taking 4-year running average.

suggests the existence of a ≈ 60 -year cycle in $\overline{\%G}$. The average values of $\overline{\%D}$ over the periods 1900–1920 and 1960–1990 seem to be somewhat larger than the corresponding averages values over the periods 1874–1900, 192–1960, and 1960–2008. Moreno-Insertis and Vázquez (1988) and Martínez Pillet, Moreno-Insertis, and Vázquez (1993) found the evidence for a significant variations in the decay rates of the spot groups of Cycles 12 through 16. We also see such an evidence in the variation of $\overline{\%D}$. In fact, one can see the following trends: an increase in $\overline{\%D}$ from 1874 to 1900 and then a decrease up to 1945, again an

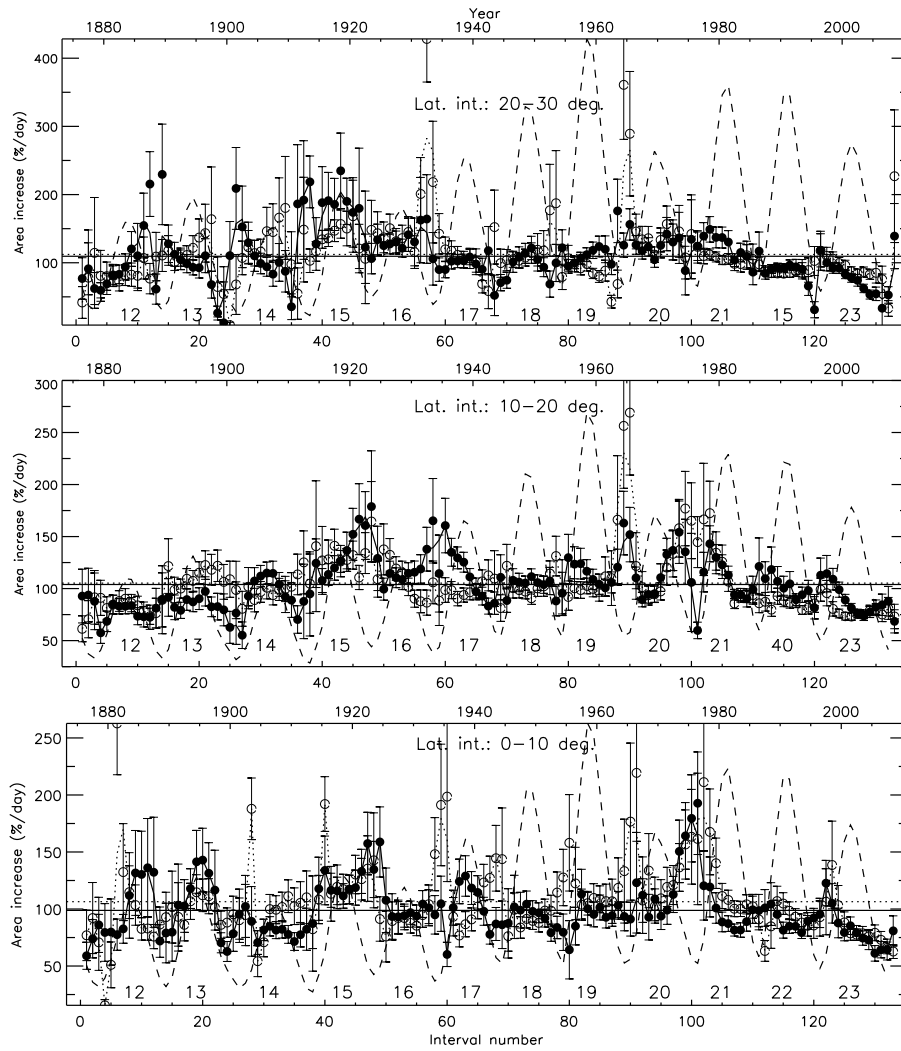


Figure 4. Same as Fig. 3a, but determined separately for different 10° latitude intervals.

increase up to 1980 and then a decrease. This pattern suggests the existence of a 60–80-year cycle in $\%D$. On the other hand, there is only a weak correlation (25%–40%) between $\%G$ and $\%D$, indicating that there may be differences in the long-term trends of the $\%G$ and $\%D$, which cannot be detected in the present analysis due to inadequate data. Overall, we find that $\%G$ varies by about 35% on a 60–80 year time scale, whereas $\%D$ seems to vary by about 13% on nearly the same time scale.

Figure 7 shows the cycle-to-cycle modulations in $\overline{\%G}$ and $\overline{\%D}$ determined by averaging the corrected annual values (shown in Figure 2) over the duration of each of the Cycles 12–23. In the same figure the variation in the amplitudes of the cycles (R_M , the largest smoothed monthly mean sunspot numbers, taken from the website, ftp://ftp.ngdc.noaa.gov/STP/SOLAR_DATA/SUNSPOT

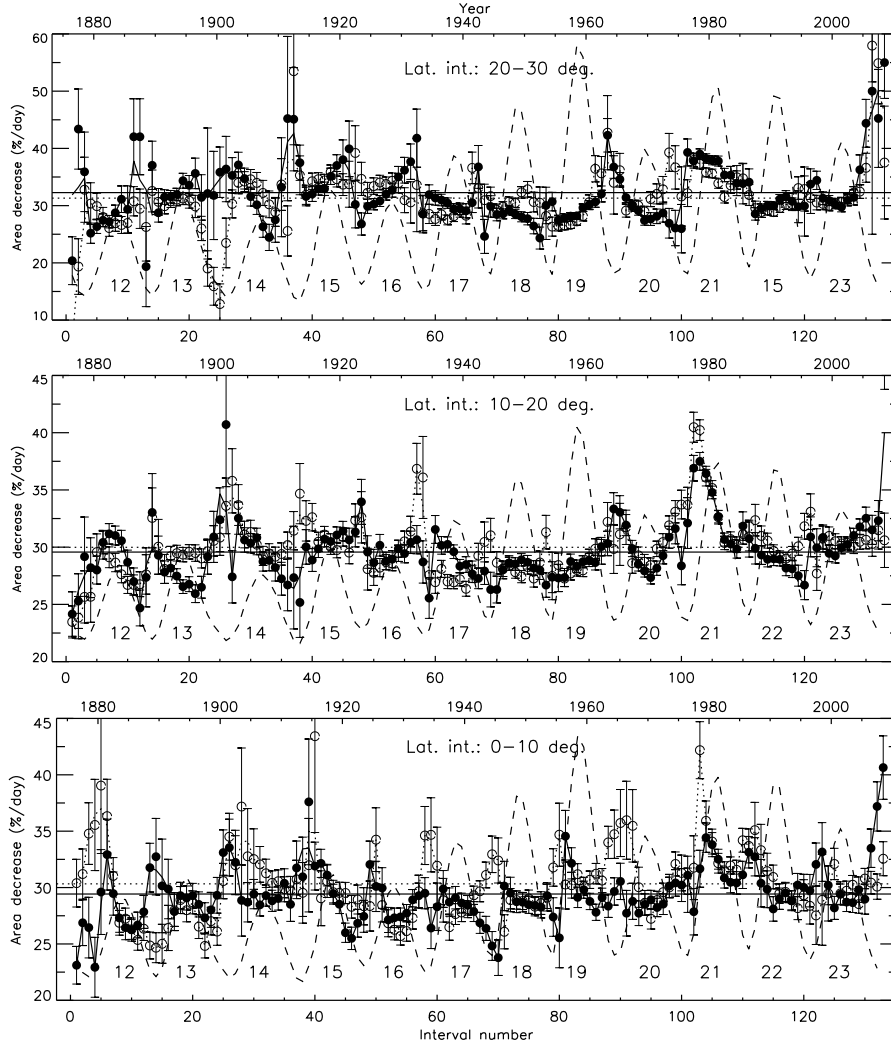


Figure 5. Same as Fig. 3b, but determined separately for different 10° latitude intervals.

NUMBERS), is also shown. From this figure one can see clearly the long-term variations described above, *i.e.*, a cycle of about 55 years in $\%G$ with minimum epoch at Cycle 18 and maximum epochs at Cycle 15 and 20, and a cycle of about 65 years in $\%D$ with minimum epoch around Cycles 18–19 and maximum epochs at Cycles 15 and 21. The correlation between $\%G$ and $\%D$ from the 12 pairs of data points is only 78%. The 10-year difference between the periods of these cycles might have caused a few year phase catastrophe and responsible for the weak correlation. There is no correlation (values are very small, 6%–12%) either between $\%G$ and R_M or between $\%D$ and R_M . In addition, $\%G$ is considerably large in the declining phases of some solar cycles and $\%D$ is considerably large in the rising phases of some cycles (see Figure 6). Therefore, the relation between the sunspot activity and the evolution rates of the spot groups is not clear. On

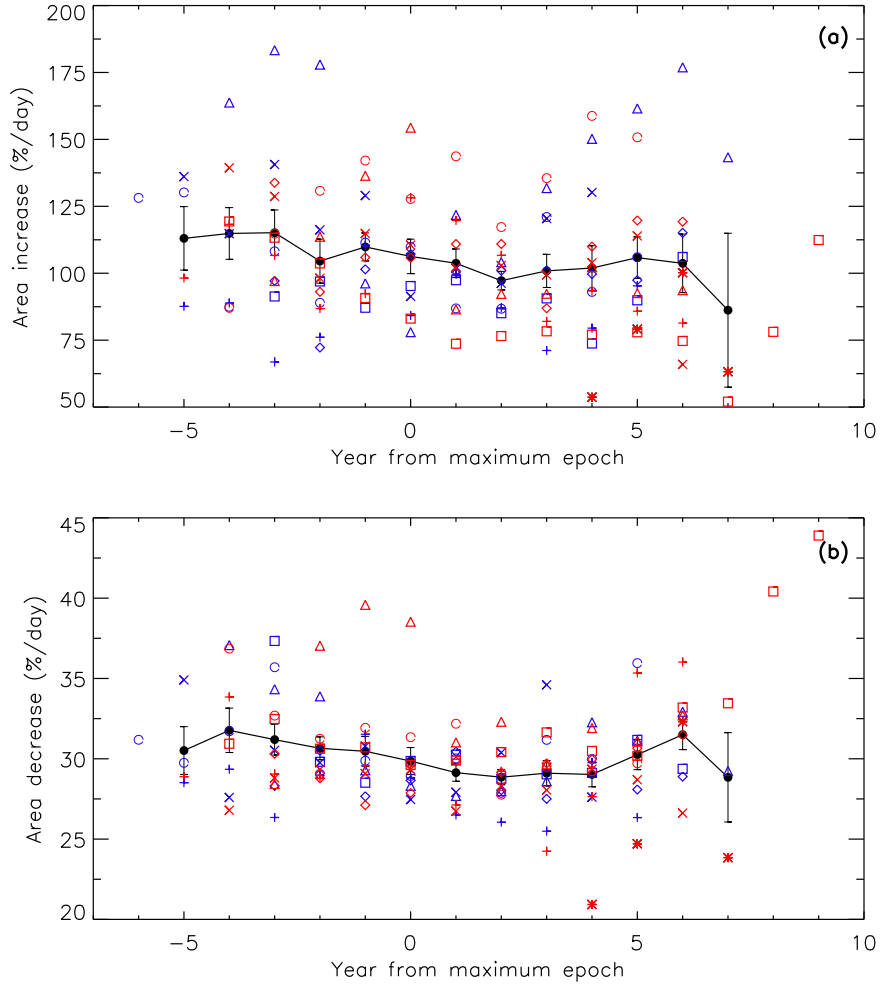


Figure 6. Plots of the yearly mean values (the corrected data points which are connected by continuous curves in Figure 2) of $\%G$ (upper panel) and $\%D$ (lower panel) versus the year from maximum epoch of the solar cycle. The red and blue colors are used for odd- and even-numbered cycles, respectively. The different symbols are used for different cycles (numbers are given in brackets): asterisks (11), pluses (12 and 13), open-circles (14 and 15), crosses (16 and 17), diamonds (18 and 19), triangles (20 and 21), and squares (22 and 23). The filled circle-continuous curve represents the mean solar cycle variation determined from the yearly mean values. The error bar represents the standard error. There is only one data point at years -6 (begin of Cycle 14), 8 (end of Cycle 23) and 9 (beginning of Cycle 24).

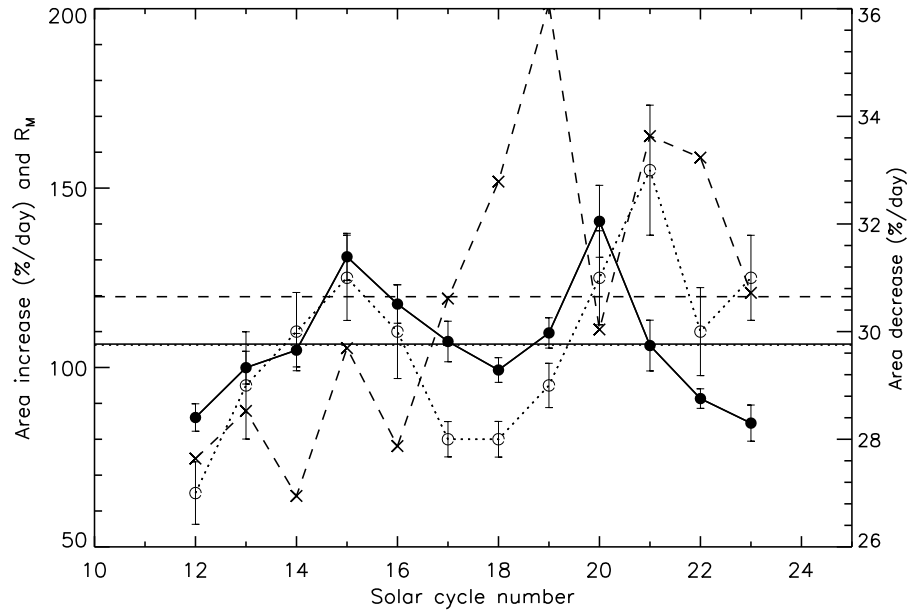


Figure 7. Cycle-to-cycle modulations in $\overline{\%G}$ (filled circle-solid curve) and $\overline{\%D}$ (open circle-dotted curve) determined by averaging (over a whole solar cycle) the corrected annual values shown in Figure 2. The error bar represents the standard error. The cross-dashed curve represents the the maximum amplitude (R_M , the largest smoothed monthly sunspot numbers) of the solar cycles. The continuous and dotted horizontal lines (they overlap) represent the average (over all 12 cycles) values 106.52 and 29.75 of $\overline{\%G}$ and $\overline{\%D}$, respectively. The dashed line represents the mean value (119.74) of R_M .

the other hand, the different types of cycles of the sub-century and the century time scales may be dominant in indices of different types of activity (Komitov *et al.*, 2010). Subsurface and surface flows may be responsible for the growth and the decay of the spot groups (active regions in general). It may be interesting to note that the correlation between the powerful flare events and sunspot number is weak and a significant 50–60-year periodicity seems to be highly pronounced in the powerful flare-related data (Komitov *et al.*, 2010). Evolution of sunspot groups may be related to the cancelation/enhancement of the subsurface/surface magnetic flux due to the reconnection process, which seems to be the main mechanism of solar flare activity. Hence, the long-term variations in $\overline{\%G}$ and $\overline{\%D}$ may be related to the corresponding long-term variations in the powerful flare events.

Although over the 12 cycles the values of the correlations between $\overline{\%G}$ and R_M , and between $\overline{\%D}$ and R_M , are small, in Figure 7 there is a suggestion that the increasing/decreasing trends of both $\overline{\%G}$ and $\overline{\%D}$ during 3–4 cycles are related to the mean R_M of the corresponding cycles, which is lower/greater than the mean R_M of the 12 cycles. In addition, the ≈ 55 –60-year cycle looks to be superposed (particularly in the case of $\overline{\%G}$) on a much stronger cycle of ≈ 120 -

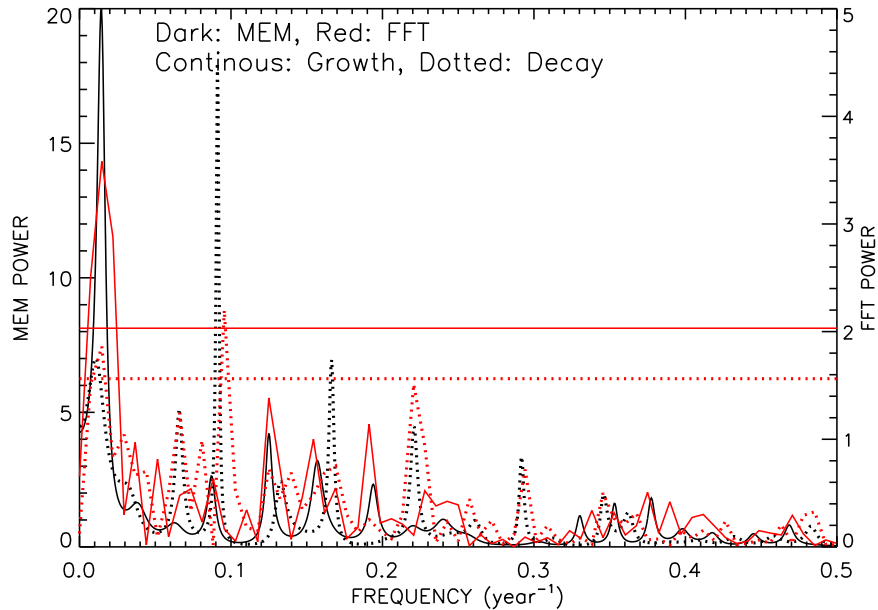


Figure 8. FFT and MEM power spectra of the corrected yearly data of $\overline{\%G}$ and $\overline{\%D}$ (whole sphere data) shown in Figure 2. The continuous and dotted horizontal lines represent the 95% confidence levels of the peaks in the corresponding FFT spectra.

year (with minima at Cycles 12 and 23). In this context it may be worth to note that the length of the current Gleissberg cycle is also substantially long, 113 ± 5 years (Javaraiah, Bertello, and Ulrich, 2005). These trends in $\overline{\%G}$ and $\overline{\%D}$ indicate that both these parameters will slightly increase during the next 2–3 cycles and the behavior may be similar to the corresponding trends of $\overline{\%G}$ and $\overline{\%D}$ during Cycle 12–15. Since, Cycles 12–15 are on the average weak cycles, hence the next few cycles may be weak cycles. This inference is also consistent with the following suggestions: (i) the violation of the G-O rule by cycle pair 22,23 might be followed by a few weak cycles (Javaraiah, 2005); (ii) now the level of activity may correspond to the declining phase of the current Gleissberg cycle (Javaraiah, Bertello, and Ulrich, 2005); and (iii) a small amplitude predicted for solar Cycle 24 (Javaraiah, 2008 and references therein).

We find the high correlations 69% and 74% between the northern and the southern hemisphere $\overline{\%G}$ and $\overline{\%D}$ shown in Figure 3, respectively, suggesting that the long-term variations in $\overline{\%G}$ and $\overline{\%D}$ are closely symmetric about the Sun's equator. However, as can be seen in Figure 3, the phases of the variations of $\overline{\%G}$ in the northern and the southern hemispheres seem to be opposite during each of the Cycles 17–19. In fact, we obtained -74% correlation from 20 pairs of data points of $\overline{\%G}$ correspond to the time number interval 65–84, *i.e.*, between around the maximum epochs of Cycles 17 and 19. On the other hand, in the recent four cycles there is no north-south asymmetry in $\overline{\%G}$, indicating that a high coherence in the variations of $\overline{\%G}$ of the northern and the southern

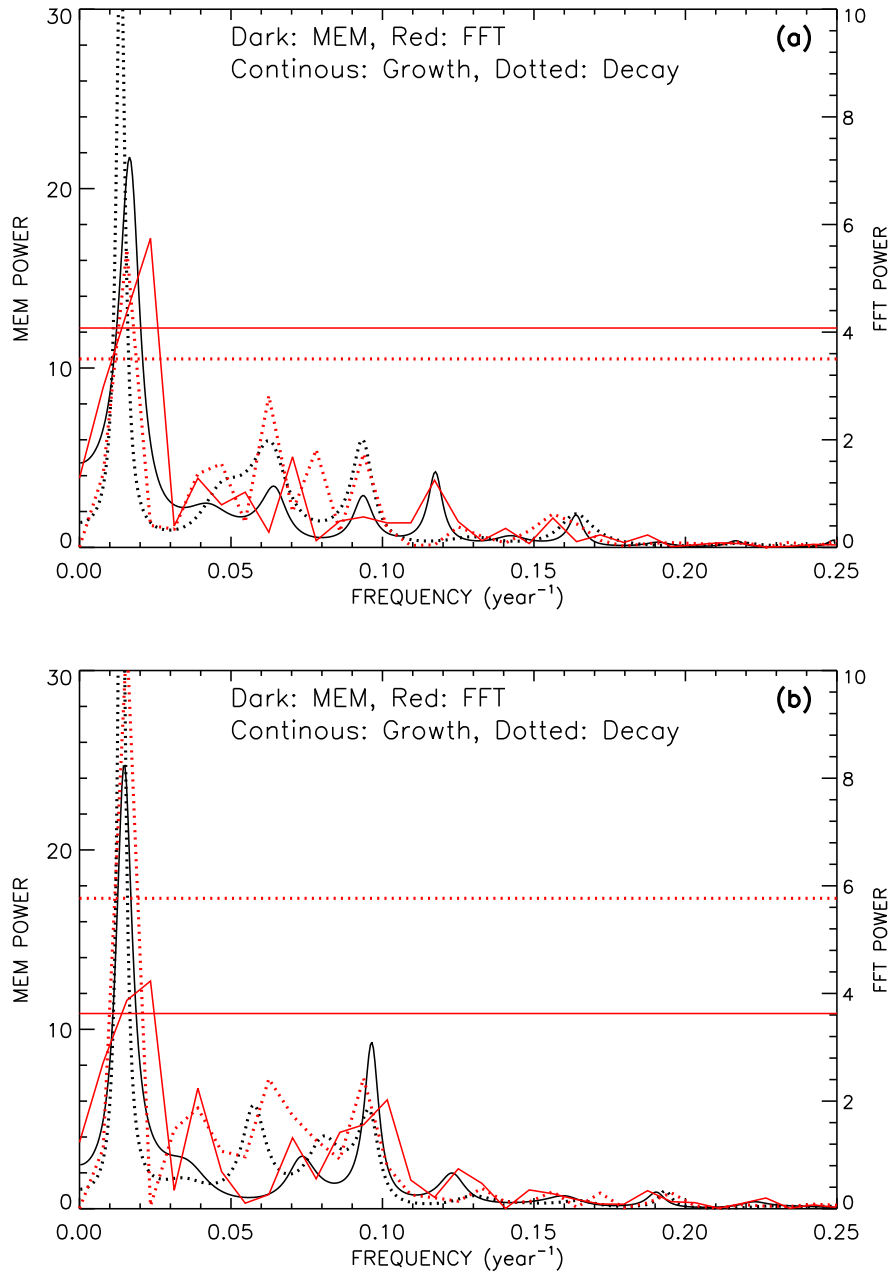


Figure 9. FFT and MEM power spectra of $\overline{\%G}$ and $\overline{\%D}$ determined (a) from the whole northern hemisphere data and (b) from the whole southern hemisphere data in 4-year MTIs shown in Figure 3.

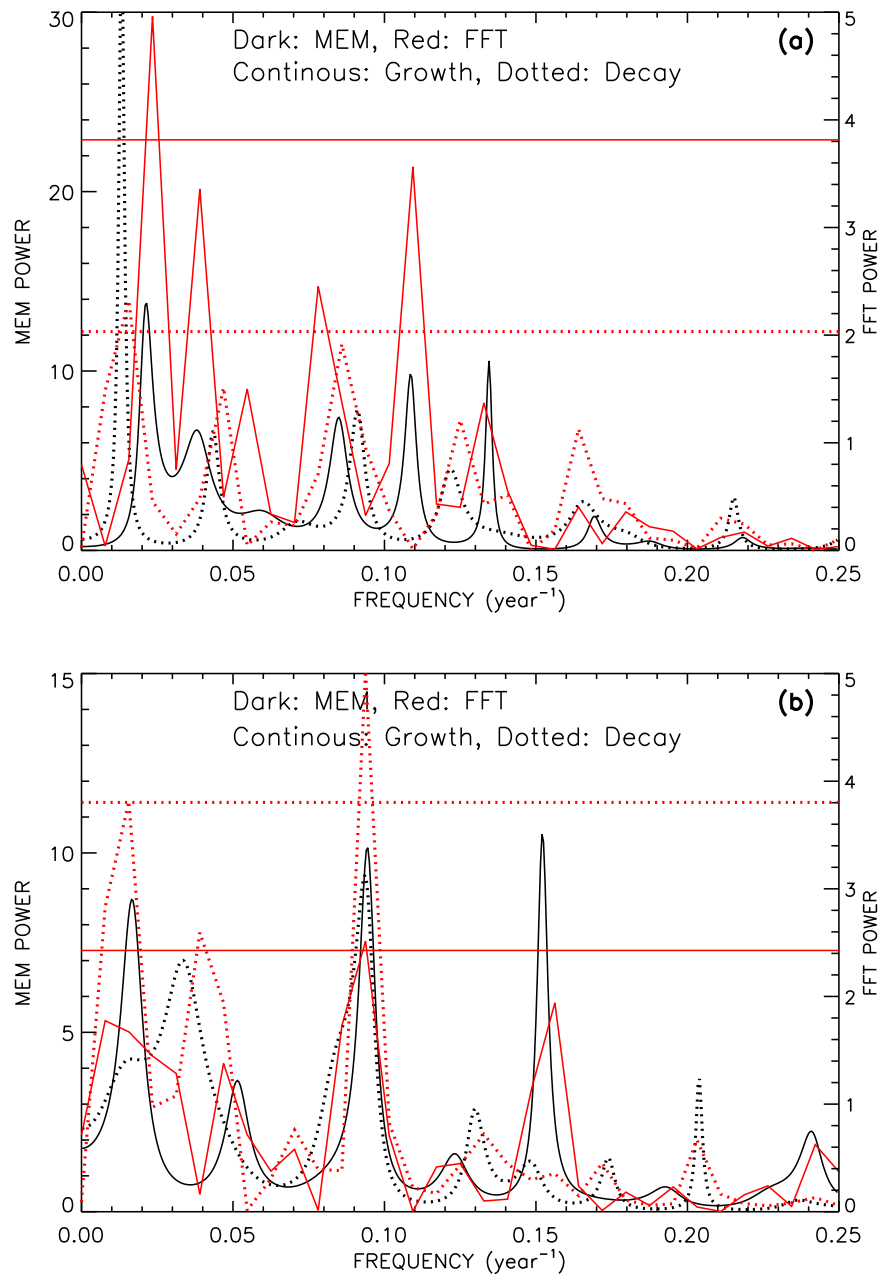


Figure 10. FFT and MEM spectra of $\overline{\%G}$ and $\overline{\%D}$ determined from the data in $0^\circ - 10^\circ$ latitude intervals of (a) the northern hemisphere and (b) the southern hemisphere, during 4-year MTIs shown in Figures 4 and 5.

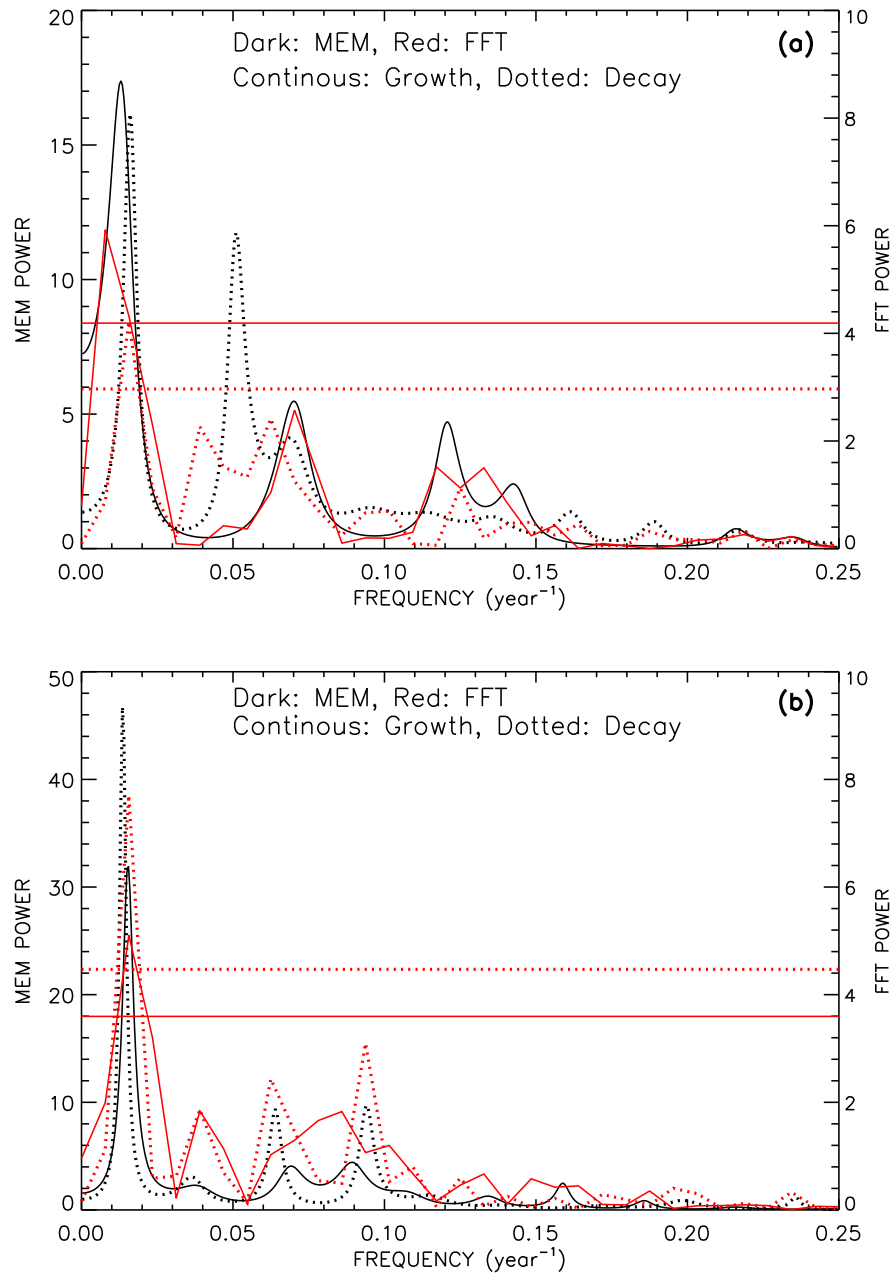


Figure 11. The same as Figure 10, but for the data in $10^\circ - 20^\circ$ latitude intervals.

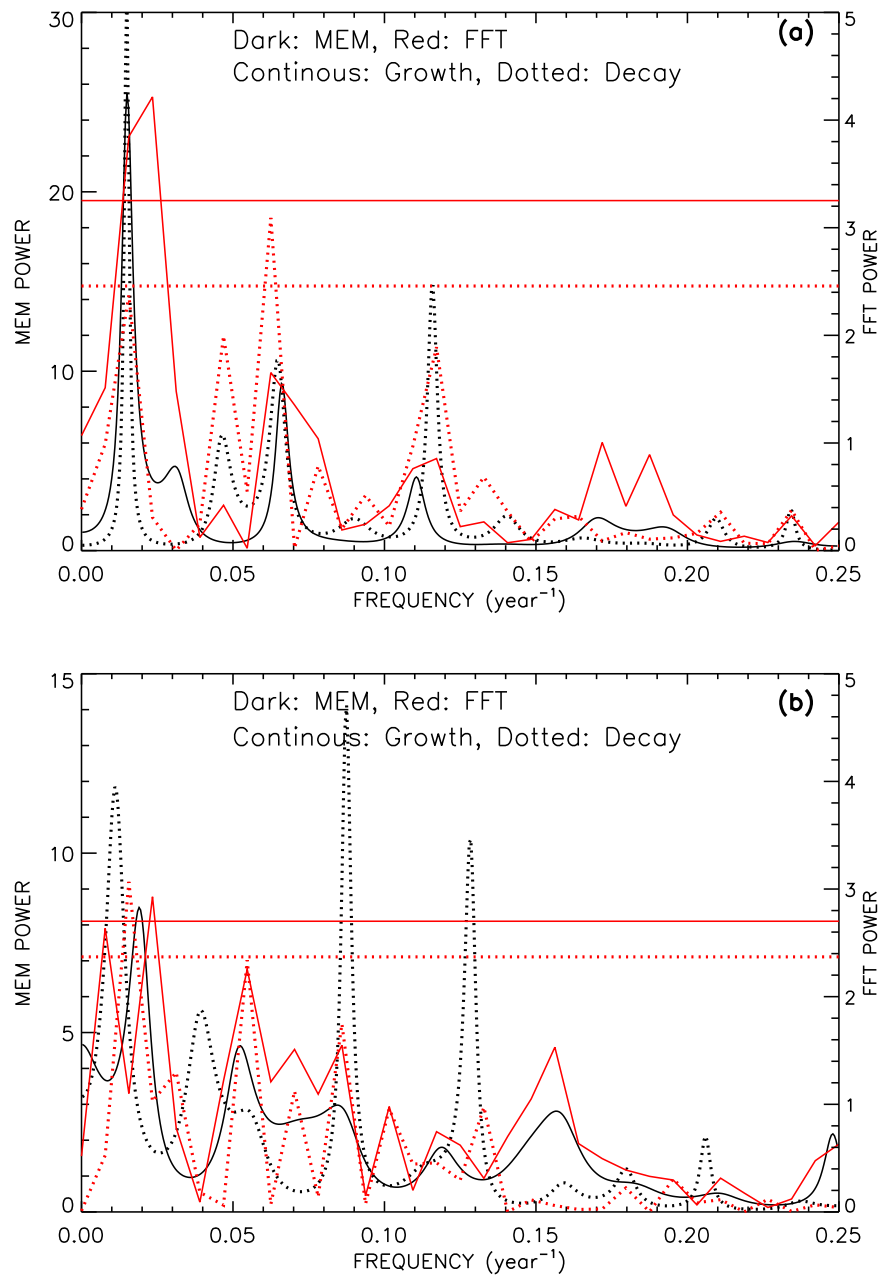


Figure 12. The same as Figure 10, but for the data in $20^\circ - 30^\circ$ latitude intervals.

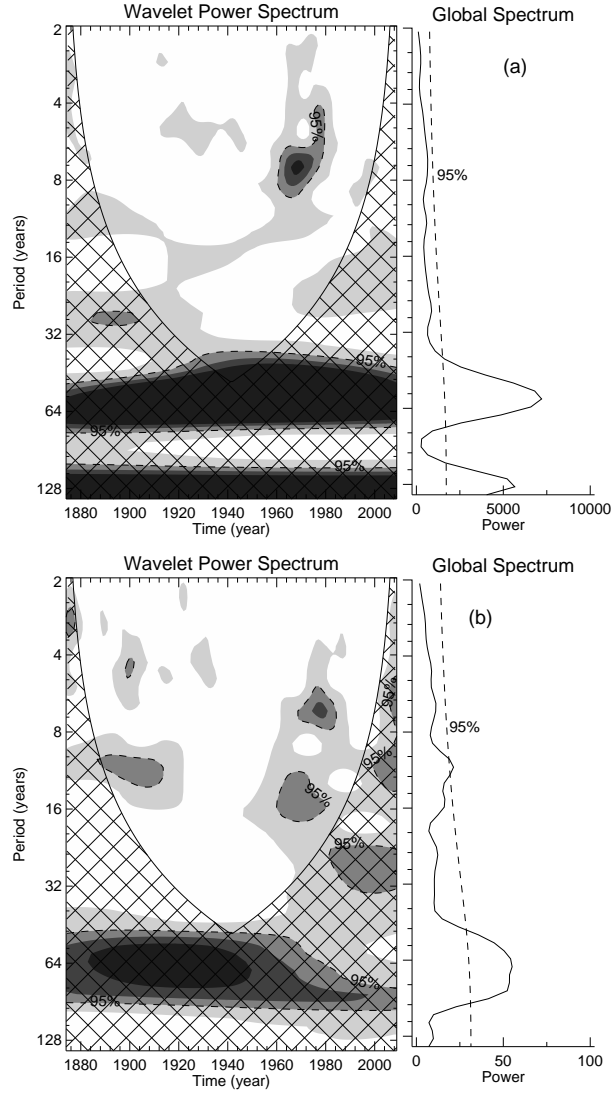


Figure 13. Wavelet power spectra and global spectra of the corrected yearly time series of $\overline{\%G}$ (upper panel) and $\overline{\%D}$ (lower panel) shown in Figure 2. The wavelet spectra are normalized by the variances of the corresponding time series. The shading are the normalized variances of 1.0, 3.0, 4.5, and 6.0, respectively. The dashed curve represents the 95% confidence level, deduced by assuming a white noise process. The cross-hatched regions indicate the "cone of influence", where edge effects become important (Torrence and Compo, 1998).

hemispheres is associated with reduced amplitude of a 33–44-year cycle (may be due to equatorial crossing of the magnetic flux in the convection zone). Thus, the strength of a 33–44-year cycle in the solar activity may be related to the strength of the north-south asymmetries in $\overline{\%G}$ during the 11-year solar cycles that comprise the 33–44-year cycle in activity. There is no north-south asymmetry in $\overline{\%D}$ throughout the period 1874–2009, except during Cycle 17.

Figures 8–12 show the FFT and the MEM power spectra of the variations in $\overline{\%G}$ and $\overline{\%D}$ shown in Figures 2–4 (the last few years data have not been used in case of all the time series of the 4-year MTIs, because their inclusion found to distort the low frequency sides of the corresponding MEM spectra). It should be noted that as the size of the time-interval increased the peaks at high frequencies are washed-out. Therefore, only low frequency sides of the spectra are shown in Figures 9–12. However, the 95% significant levels of the peaks in the FFT spectra are determined by considering only the power at these low frequencies. (Note: the spectra which correspond to the $20^\circ - 30^\circ$ latitude interval are less reliable due the scarcity of the data in many 4-year time-intervals.) Most of these spectra show the existence of a 60–80-year periodicity in both $\overline{\%G}$ and $\overline{\%D}$, with the corresponding peaks in the FFT spectra are about 95% confidence level. (The MEM spectra of the yearly data of $\overline{\%G}$ and $\overline{\%D}$ yield the values 59-year and 71-year, respectively, for the 60–80-year periodicity.) In addition, the following peaks at frequencies which are close to the solar cycle frequency are significant on $\geq 95\%$ confidence level: (i) the peak at frequency $\approx 0.1 \text{ year}^{-1}$ in the FFT spectra of both $\overline{\%G}$ and $\overline{\%D}$ of $0^\circ - 10^\circ$ latitude interval of the southern hemisphere (see Figure 10(b)); and (ii) the peak at frequency $\approx 0.055 \text{ year}^{-1}$ in the FFT spectrum of $\overline{\%D}$ of $20^\circ - 30^\circ$ latitude interval of the northern hemisphere (see Figure 12(a)). These results suggest that the periodicities which are close to the solar cycle period are time and latitude dependent. Figure 13 shows the wavelet spectra of the corrected time series shown in Figure 2. The lengths of the time series are inadequate to resolve the temporal dependency of 60–80-year periodicity. The periodicities of $\overline{\%D}$ which are close to the solar-cycle period seem to have occurred during the period 1900–1920 and around the period 1975–1995. A 7–8-year periodicity in $\overline{\%G}$ and also in $\overline{\%D}$ seems to occur during the period 1960–1980. A ≈ 5 -year periodicity in $\overline{\%D}$ occurred around 1900.

Hathaway and Chowdhury (2008) noted that the solar cycle variation in the decay rates of the spot groups is merely coming from the latitude-time distribution of the spot groups. The existence of a 90-year cycle is also found in the widths of the Butterfly diagram (Pulkkinen *et al.*, 1999). Therefore, one can suspect that the long-term (≈ 60 -year) periodicity found here in $\overline{\%G}$ and $\overline{\%D}$ may also be artifacts of the long-term variations in the width of the Butterfly wings. On the other hand, in Figures 4 and 5 we can see that all the above said properties in the variations of $\overline{\%G}$ and $\overline{\%D}$ are present in each of the 10° latitude intervals, though the patterns are not as well defined as those of $\overline{\%G}$ and $\overline{\%D}$ in a whole hemisphere. However, a large contribution to the 60–80-year variations in $\overline{\%G}$ and $\overline{\%D}$ of a whole hemisphere is came from the corresponding variations in the $10^\circ - 20^\circ$ latitude interval (see Figure 11).

4. Discussion and Conclusions

The following conclusions can be drawn from the above analysis:

1. The minimum and the maximum values of the annual mean growth rates of the spot groups are $\approx 52\% \text{ day}^{-1}$ and $\approx 183\% \text{ day}^{-1}$, respectively, whereas the corresponding values of the annual mean decay rates are $\approx 21\% \text{ day}^{-1}$ and $\approx 44\% \text{ day}^{-1}$, respectively. The average value (over the period 1874–2009) of the daily growth rate is about 70% more than that of the decay rate.
2. The growth and the decay rates vary by about 35% and 13%, respectively, on a 60-year time scale.
3. A ≈ 11 -year periodicity in the growth and the decay rates is found to be highly latitude and time dependent and seems to exist in both the growth and the decay rates of the spot groups mainly in the $0^\circ - 10^\circ$ latitude interval of the southern hemisphere.
4. From the beginning of Cycle 23 the growth rate is substantially decreased and near the end (2007–2008) the growth rate is lowest in the past about 100 years. In the extended part (beyond the length of the declining part of a normal cycle) of the declining phase of this cycle, the decay rate steeply increased and it is largest in the beginning of the current Cycle 24. These unusual properties of the growth and the decay rates during Cycle 23 may be related to the very long declining phase of this cycle with the unusually deep and prolonged current minimum.
5. The strength of the known approximate 33–44 year modulation in solar activity seems to be related to the strength of the north-south asymmetry in the growth rate during the 11-year solar cycles that comprise the 33–44 year cycle in activity.
6. Decreasing and increasing trends in the growth and the decay rates indicate that the next 2–3 solar cycle will be relatively weak.

The conclusions (1) and (2) above, *i.e.*, the lower decay rate and its slow evolution support the idea of a long-term persistence of the solar activity. This is consistent with an hypothesis of some class of turbulent dynamo models (Dikpati and Gilman, 2006), although the present analysis (conclusion 6, above) does not support the large amplitude for the current Cycle 24 that is predicted in these models.

The existence of a quasi-periodic long-term variation (Gleissberg cycle) in solar activity is well known. However, a wide range of values (50–130 years) are suggested for Gleissberg cycle. Among them the existence of 60–80-year periodicity is frequently reported (Komitov *et al.*, 2010). The 60–80-year cycles of the growth and decay rates may be related to the corresponding cycles in the powerful flare events, rather than to that of the sunspot activity (see previous section).

One can expect that convection has a major role in the day-to-day fluctuations of the areas of spot groups. The growth and decay of an active region may have an association with upward flow and the reverse down flow of the convection, respectively (see also Komm, Howe, and Hill, 2009). The long-term variations in the day-to-day fluctuations in the areas of the spot groups largely represent

the corresponding long-term variations in the convective flows. The long-term variation in the convection may be related to the corresponding long period global oscillation of the Sun.

Acknowledgements The author thanks the anonymous referee for useful comments and suggestions. Wavelet software was provided by Ch. Torrence and G.P. Compo, and is available at URL: <http://poas.colorado.edu/research/wavelets/>. The MEM FORTRAN code was provided to us by Dr. A.V. Raveendran.

References

- Berryman, J.G.: 1978, *Geophys.* **43**, 1384.
 Dikpati, M., Gilman, P.A.: 2006, *Astrophys. J.* **649**, 498.
 Gough, D.O.: 2010, in Magnetic Coupling between the Interior and the Atmosphere of the Sun, eds. S. S. Hasan & R. J. Rutten, *Astrophys. Space Sci. Proc.* **SSA 1570-6591**, Springer-Verlag Berlin Heidelberg, 37.
 Hathaway, D.H., Choudhary, D.P.: 2008, *Solar Phys.* **250**, 269.
 Howard, R.F.: 1992a, *Solar Phys.* **137**, 51.
 Howard, R.F.: 1992b, *Solar Phys.* **142**, 47.
 Javaraiah, J.: 2005, *Mon. Not. Roy. Astron. Soc.* **362**, 1311.
 Javaraiah, J.: 2008, *Solar Phys.* , 252, 419.
 Javaraiah, J.: 2010, *Astron. Astrophys.* **509**, A30.
 Javaraiah, J., Bertello, L., Ulrich, R.K.: 2005, *Solar Phys.* **232**, 25.
 Javaraiah, J., Gokhale, M.H.: 1995, *Solar Phys.* **158**, 173.
 Komitov, B., Sello, S., Duchlev, P., Dechev, M., Penev, K., and Koleva, K.: 2010, arXiv:1007.3143v1 [astro-ph.SR]
 Komm, R., Howe, R., Hill, F.: 2009, *Solar Phys.* **258**, 13.
 Lustig, G., Wöhl, H.: 1995, *Solar Phys.* **157**, 389.
 Martínez Pillet, V., Moreno-Insertis, F., Vázquez, M.: 1993, *Astron. Astrophys.* **274**, 521.
 Moreno-Insertis, F., Vázquez, M.: 1988, *Astron. Astrophys.* **205**, 289.
 Pulkkinen, P.J., Brooke, J., Pelt, J., Tuominen, I.: 1999, *Astron. Astrophys.* **341**, L43.
 Rosner, R., Weiss, N.O.: 1992, In: Harvey, K.L. (ed.) *The Solar Cycle*, **CS-27**, *Astron. Soc. Pac.*, San Francisco, 511.
 Torrence, Ch., Compo, G.P.: 1998, *Bull. Am. Meteor. Soc.* **79**, 61.
 Ulrych, T. J., Bishop, T.N.: 1975, *Rev. Geophys. Space Phys.*, **13**, 183.
 Wang, Y.-M., Sheeley, N.R., Jr.: 1989, *Solar Phys.*, 124, 81.
 Ward, F.: 1966, *Astrophys. J.* **145**, 416.